Analyst

Accepted Manuscript

This article can be cited before page numbers have been issued, to do this please use: D. Thirumalai, V. Kathiresan, J. Lee, S. Jin and S. Chang, *Analyst*, 2017, DOI: 10.1039/C7AN01387F.

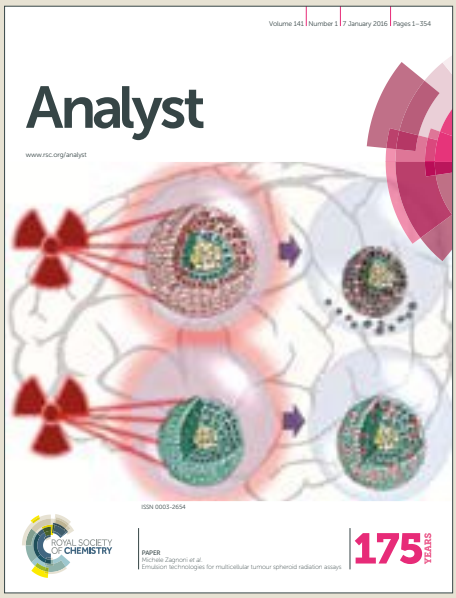

ROYAL SOCIETY OF CHEMISTRY

rsc.li/analyst

View Article Online
DOI: 10.1039/C7AN01387F

Electrochemical reactive oxygen species detection by cytochrome *c* immobilized with vertically aligned and electrochemically reduced graphene oxide on glassy carbon electrode

Dinakaran Thirumalai[a], Vijayaraj Kathiresan[a], Jaewon Lee[b], Sung Ho Jin[a,c] and Seung-Cheol Chang[d,*]

[a]Graduate Department of Chemical Materials, Pusan National University, Busan 46241, Republic of Korea

[b]College of Pharmacy, Molecular Inflammation Research Center for Aging Intervention, Pusan National University, Busan 46241, Republic of Korea

[c]Department of Chemical Education, Pusan National University, Busan 46241, Republic of Korea

[d]Institute of Bio-Physio Sensor Technology, Pusan National University, Busan 46241, Republic of Korea

E-mail: s.c.chang@pusan.ac.kr

View Article Online
DOI: 10.1039/C7AN01387F

Abstract

A new amperometric biosensor for hydrogen peroxide (H_2O_2) and superoxide anion (SO) has been developed. The biosensor developed uses cytochrome *c* (Cyt *c*) modified glassy carbon electrodes coupled with electrochemically reduced graphene oxide (ErGO). To immobilize Cyt *c*, the "one step" electrochemical deposition of vertically aligned and ErGO (VAErGO) has been performed by using a pulse reverse technique, thus resulting in a very simple and efficient system. The well-established vertical alignment of ErGO was confirmed by atomic force microscopy and the electrochemical characteristics of the biosensor were investigated by cyclic voltammetric, electrochemical impedance spectroscopy and amperometric techniques. The surface coverage (Γ) of immobilized Cyt *c* was effectively increased by the vertical alignment of ErGO and found to be 1.03×10^{-10} mol·cm^{-2}. The direct electron transfer property of Cyt *c* was also improved by VAErGO and the heterogeneous electron transfer rate constant (k_{et}) was estimated to be 6.40 s^{-1}. To detect H_2O_2 and SO, amperometric measurements were carried out at different operating potentials (0.0 V *vs.* Ag/AgCl for H_2O_2 and +0.2 V for SO). The sensitivity and detection limit for H_2O_2 were found to be 46.3 μA·mM^{-1}·cm^{-2} and 2.3 μM, and for SO were found to be 32.1 μM ·nA^{-1}·cm^{-2} and 6.84 nM·s^{-1}, respectively. Additionally, the designed biosensor exhibited strong anti-interference ability and satisfactory reproducibility.

View Article Online
DOI: 10.1039/C7AN01387F

Introduction

Reactive oxygen species (ROS) are unavoidable by-products of aerobic cell metabolism. ROS function as physiological regulators of intracellular signaling pathways.[1, 2] Superoxide anion radical (SO), hydroxyl radical ($OH^{\cdot}$), singlet oxygen ($^1O_2$), and hydrogen peroxide (H_2O_2) are well-known examples of ROS. Several ROS are radicals and highly toxic. The radicals induce either programmed cell death (apoptosis) or un-programmed cell death (necrosis) through oxidation of biomolecules. Under normal physiological conditions, anti-oxidants function to control intracellular ROS levels by multiple steps of both enzymatic and non-enzymatic detoxification processes. Deficiencies or defects in the anti-oxidant defense system could result in the production of ROS that exceed their catabolism and create oxidative stresses.[3, 4] Excess ROS has been implicated in various pathological diseases such as different types of cancers, neurological disorders, cardiovascular diseases, ischemia, diabetes mellitus, as well as the aging process.[5, 6]

In clinical and biochemical research, monitoring or measuring ROS-associated biological function is crucial to evaluate the effect of therapies. However, ROS have very short half-lives, are highly reactive, and exist *in vivo* in a variety of anti-oxidant forms that make them difficult to detect. To overcome these difficulties, spectroscopic techniques such as fluorescence, electron spin resonance and chemiluminescence have been applied to monitor ROS production.[7-9] Hence, the abovementioned techniques have their own limitations, such as low cost effectiveness, expensive instrumentation, lengthy sample preparation procedures, and less selectivity and specificity. Therefore, electrochemical biosensor systems are a logical choice for ROS detection

View Article Online
DOI: 10.1039/C7AN01387F

because of their high portability and cost effectiveness, and applicability for real time *in vitro* and *in vivo* measurements.[10-12]

Heme-containing proteins such as cytochrome *c* (Cyt *c*), myoglobin (Mb) and hemoglobin (Hb) are capable of catalyzing the reduction of ROS.[13, 14] Cyt *c* is a small redox protein containing 104 amino acids and is the most widely studied protein in electrochemical applications.[15] The immobilization of Cyt *c* onto solid (electrode) surfaces greatly influences their biological activities and properties, which is of great importance in biosensor fabrication. On bare electrode surfaces, Cyt *c* activity is generally poor and irreversible.[16] Therefore, to enhance the biological activity and stability, various supporting nanomaterials have been used for immobilization of Cyt *c* such as colloidal gold,[17] gold nanoparticles,[18] nickel oxide nanoparticles,[19] zinc oxide nanosheets,[20] polymers,[21] carbon nanotubes,[22] and graphene.[21, 23, 24] Among these studies, only two immobilization strategies have been used namely physical (adsorption) and covalent (amine chemistry) methods. However, the physical method may cause Cyt *c* detachment from the electrode surface due to the random orientation and weak attachment of the protein. In the covalent method, by contrast, Cyt *c* can be effectively immobilized onto the supporting nanomaterials by stable covalent bonding.

In the present study, we propose a new "one-step" covalent immobilization method of Cyt *c* onto a glassy carbon electrode (GCE) by using a pulse reverse technique to co-deposit Cyt *c* with graphene oxide. The amine groups of the lysine residues on Cyt *c* reacted with carboxyl functional group via the formation of covalent amide (-CO-NH-) bonding and the reaction was performed using *N*-(3-dimethylaminopropyl)-*N(3*ethylcarbodiimide hydrochloride (EDC) and *N*-hydroxy succinimide (NHS). Subsequently, the electrochemical reduction of graphene oxide

View Article Online
DOI: 10.1039/C7AN01387F

resulted in the simultaneous deposition of Cyt *c* and formed vertically aligned electrochemically reduced graphene oxide (VAErGO). The proposed electrode has been used to investigate the direct electron transfer (DET) property and the peroxidase-like activity of Cyt *c,* and the biosensors constructed have been used to detect H_2O_2 and SO (Scheme 1).

Experimental

Materials

Cyt *c* from equine heart, *N*-(3-dimethylaminopropyl)-*N(3*ethylcarbodiimide hydrochloride (EDC), *N*-hydroxysuccinimide (NHS), 5 wt.% Nafion (Nf), xanthine (XA), xanthine oxidase (XOD, EC 1.17.3.2) from bovine milk, potassium ferricyanide $K_3[Fe(CN)_6]$, potassium chloride (KCl), indium tin oxide (ITO) coated glass and graphite flakes were purchased from Sigma-Aldrich (USA). All other chemicals were of analytical grade and used without further purification. Phosphate-buffered solution (PBS, 0.1 M) was prepared by mixing sodium phosphate monobasic (NaH_2PO_4) with sodium phosphate dibasic (Na_2HPO_4) and used as a working buffer. All aqueous solutions were prepared in deionized water, which was obtained from a Milli-Q® water purifying system (18 MΩ·cm^{-1}) (EMD Millipore, USA).

"One-step" immobilization of Cyt *c*

Graphene oxide (GO) was synthesized according to a modified Hummers method,[25] and the resulting solid brown powder was ultrasonically exfoliated in distilled water for 1 h to disperse the GO. A volume of 0.8 mg·mL^{-1} GO was mixed with 2 mM EDC and 5 mM NHS in 10 mL of PBS (0.1 M) at pH 6.0 and stirred for 5 min at room temperature. Subsequently, 50 µM Cyt *c* was added and mixed well. The resulting colloidal suspension was incubated at 4 °C in a refrigerator overnight for the formation of amide bonding between Cyt *c* and GO.

View Article Online
DOI: 10.1039/C7AN01387F

Prior to electrochemical co-deposition, the GCE was polished with 0.3 μm alumina powder and thoroughly rinsed with ethanol and distilled water. The electrochemical co-deposition was carried out using a pulse reverse electrodeposition technique.[26, 27] The GCE was immersed in a colloidal suspension of GO with Cyt *c* and deposited under stirring. The parameters of the electrodeposition process, such as anodic pulse potential +0.6 V and pulse duration 0.3 s, cathodic pulse potential −1.3 V and pulse duration 0.6 s for 400 cycles (total time 360 s) were applied. After electrochemical deposition, the resulting Cyt *c*–VAErGO/GCE was rinsed with distilled water and air-dried at room temperature. Finally, 1 μL of Nf (0.5 wt.%) was drop-casted and air dried at room temperature to obtain the Nf/Cyt *c*–VAErGO/GCE. For the control, 0.8 $mg \cdot mL^{-1}$ of GO was dispersed in 10 mL of PBS (0.1 M) at pH 6.0 and electrodeposited by following the same procedure to obtain the Nf/VAErGO/GCE. The modified electrodes were washed with PBS and stored at 4 °C until the use.

Apparatus and measurements

The topography of the VAErGO/ITO and the Cyt *c*–VAErGO/ITO were characterized by atomic force microscopy (AFM) in the non-contact mode of operation (NX10, Park System, Corp., South Korea). Field emission scanning electron microscopy (FE-SEM) was performed using an FE-SEM S-4700 microscope (Hitachi, Tokyo, Japan). Cyclic voltammetry and electrochemical impedance spectroscopy (EIS) were performed on an electrochemical workstation (VersaSTAT 3, Princeton Applied Research, USA), and amperometric measurements were carried out with a potentiostat (Compactstat, Ivium Technologies, USA). A conventional three-electrode cell was used with a GCE (dia. 3 mm), Ag/AgCl (saturated NaCl), and a platinum wire as working, reference and counter electrodes, respectively.

View Article Online
DOI: 10.1039/C7AN01387F

The electrochemical behavior of immobilized Cyt *c* was investigated using cyclic voltammetric experiments performed in a 2 mL-volume disposable electrochemical cell with the biosensors (Nf/Cyt *c*–VAErGO/GCEs). A volume of 1 mL of PBS (0.1 M, pH 7.0) was saturated with N_2 for 20 min and the biosensors were immersed in the PBS. Cyclic voltammograms were obtained by potential sweeping from +0.6 V to −0.1 V at a scan rate of 100 $mV \cdot s^{-1}$. Amperometric measurements were performed with the biosensors. A biosensor was inserted into the electrochemical cell and connected to a potentiostat. A 900-μL aliquot of PBS (0.1 M, pH 7.0) was added to the cell and the biosensor was polarized at a potential of 0.0 V. After achieving a stable baseline response with PBS, a 100 μL aliquot of H_2O_2 samples was added to the cell and the current response was recorded as a function of time. The measurement was repeated to construct calibration curves. For the detection of SO, amperometric measurements were repeated as described except for the applied potential (0.2 V) and SO was generated by the enzymatic reaction of XOD and XA. Concentrations of SO were varied by adding various concentration of XOD into 0.1 M PBS (pH 7.0) containing 100 μM XA. For each measurement, 1.0 mM XA stock solution was freshly prepared and used. Briefly, 7.6 mg of XA was dissolved in 1.0 mL of 1.0 N NaOH and then diluted to 50 mL using 0.1 M NaH_2PO_4. The pH of the XA solution prepared was adjusted to 7.0 using 1.0 N NaOH.[28] The EIS was carried out in 0.1 M KCl containing 5 mM $[Fe(CN)_6]^{3-}$ in the frequency range from 100 kHz to 0.1 Hz at an AC potential of amplitude 5 mV superimposed on DC potential of 250 mV, which is the formal potential of the $[Fe(CN)_6]^{3-}$ redox reaction. The obtained impedance data could be fitted by Randles circuits: R[Q(RW)] for the bare GCE, and R(Q[RQ(RW)]) for the VAErGO/GCE and the Cyt *c*–VAErGO/GCE.

View Article Online
DOI: 10.1039/C7AN01387F

Results and discussion

Physical and electrochemical characterizations of VAErGO and Cyt *c*–VAErGO

AFM measurements were carried out to investigate the morphology of VAErGO and VAErGO with Cyt *c*. As shown in Fig. 1, typical AFM 3D images of VAErGO illustrate that the VAErGO stands roughly vertical to the substrate with a height profile of ca. 50 nm and a few layers of ErGO that can be horizontally covered on the substrate[31] (Fig. 1A and 1C). The AFM images of Cyt *c*–VAErGO show vertically aligned narrow peaks and islands on the substrate (Fig. 1B and 1D). These images suggested that the islands could be formed by covalent bindings between Cyt *c* and ErGO and the vertically aligned peaks could be formed by ErGO only. The height profile of the islands was calculated to be ca. 20 nm.

To characterize the electrochemical deposition of VAErGO, the cyclic voltammetric measurements were carried out using the VAErGO/GCE and compared with that of a bare GCE. As can be seen in Fig. S1, the VAErGO/GCE clearly shows an enhanced redox peak current and a slightly narrower peak-to-peak separation (ΔE_p) of 5 mM $[Fe(CN)_6]^{3-}$ prepared in 0.1 M KCl. These results obtained are attributed to a larger surface area and the facile heterogeneous electron transfer properties of VAErGO.[29] To explore the electroactive surface area of the VAErGO/GCE and the bare GCE, cyclic voltammetric measurements were repeated at different scan rates from 10 $mV \cdot s^{-1}$ to 200 $mV \cdot s^{-1}$ (Fig. S2). The electroactive surface area of the VAErGO/GCE was calculated to be 0.14 cm^{-2} by using the Randles–Sevcik equation[30] and showed two times higher than that of the bare GCE.

To investigate the co-deposition process of Cyt *c* with ErGO, FE-SEM and EIS were performed. The FE-SEM images of VAErGO and Cyt *c*–VAErGO are shown in Fig. 2. The accordion-like thin and wrinkled morphology of the graphene layers were observed in the

View Article Online
DOI: 10.1039/C7AN01387F

VAErGO image (Fig. 2A) and the graphene layers agglomeration was spotted in the few regions after the binding with Cyt *c* (Fig. 2B), indicating the effective co-deposition of Cyt *c*. The Nyquist plots from EIS experiments are shown in Fig. 2C. An appropriate Randles circuits were used to fit the obtained EIS data. The data included a semi-circular part at higher frequencies and a linear part at lower frequencies, corresponding to the charge transfer resistance (R_{ct}) limited process and to the diffusion process described by the Warburg impedance model (Z_w), respectively. When VAErGO was modified on the surface of a GCE, the R_{ct} value (44.7 Ω) was decreased as compared with the R_{ct} value of the bare GCE (87.6 Ω). This results suggest that VAErGO possesses an ability to accelerate electron transfer from $[Fe(CN)_6]^{3-}$ to electrode. The Cyt *c*–VAErGO/GCE had an R_{ct} value of 25.6 Ω, which is lower than that of the VAErGO/GCE. This might be due to an enhanced electrostatic attraction between the redox probe and positively charged Cyt *c* on the electrode surface.

DET property of immobilized Cyt *c*

In order to investigate the DET property of immobilized Cyt *c*, cyclic voltammetry was carried out with N_2-saturated 0.1 M PBS (pH 7.0) by using three differently modified electrodes: bare GCE, Nf/VAErGO/GCE, and Nf/Cyt *c*–VAErGO/GCE. As shown in Fig. 3A, a significant faradaic redox peak current was only observed on the Nf/Cyt *c*–VAErGO/GCE and the peak potentials were calculated (E_{pa}: 183 mV and E_{pc}: 123 mV) for the Fe^{III}/Fe^{II} redox couple of Cyt *c* with the ΔE_p of 60 mV at the scan rate of 100 $mV \cdot s^{-1}$. The ratio of anodic to cathodic peak current (i_{pa}/i_{pc}) was close to 1, corresponding to a reversible one electron transfer process. The mean value of peak potentials from immobilized Cyt *c* was found to be 153 mV, which is slightly shifted from the formal potential ($E°'$) of native Cyt *c* in a neutral solution (70 mV). It is well-known that the $E°'$ can be varied with temperature, pressure, electrolyte composition, and

View Article Online
DOI: 10.1039/C7AN01387F

ionic strength.[32] Additional cyclic voltammetric experiments were repeated using the Nf/Cyt *c*–VAErGO/GCE at various scan rates ranged from 25 $mV \cdot s^{-1}$ to 200 $mV \cdot s^{-1}$ (Fig. 3B). Peak currents obtained and the surface coverage (Γ) of Cyt *c* were estimated using Laviron's equation.[33] The calculated Γ value was found to be 1.03×10^{-10} $mol \cdot cm^{-2}$ and this was higher than the theoretical monolayer coverage (1.4×10^{-12} $mol \cdot cm^{-2}$)[34] and the charge value (Q) of Cyt *c* was calculated to be 6.93×10^{-7} *C*. The ca. 100 times higher Γ value clearly indicates that the vertical alignment of ErGO enhances Cyt *c* loading on the electrode surface. The Γ and Q values are comparatively three times higher than that of the Cyt *c*–ErGO/GCE prepared without EDC-NHS coupling (i.e. excluding the vertical alignment process), which also indicates that the EDC-NHS coupling (i.e. the vertical alignment process) improves the binding between GO and Cyt *c*. The k_{et} value is calculated to be 6.4 s^{-1} (the calculation details are in ESI) and compared with other studies reported previously: Cyt *c* immobilized on graphene (1.6 s^{-1}),[35] multi walled carbon nanotubes (3.6 s^{-1}),[36] and graphene-carbon nanotube composite (3.4 s^{-1}).[37] The increased k_{et} value could be caused by the vertical alignment of ErGO and it enhanced DET process between Cyt *c* and the GCE.

Peroxidase-like activity of immobilized Cyt *c*

The Cyt *c* not only possesses electro-catalytic activity, but also has an intrinsic peroxidase-like activity towards the H_2O_2 due to the structural similarities of Cyt *c* with the peroxidases family.[38] Therefore, the peroxidase-like activity of immobilized Cyt *c* was investigated by performing cyclic voltammetric measurements using the three differently modified electrodes as described. As shown in Fig. 4, any detectable peak changes in voltammograms obtained from the bare GCE and the Nf/VAErGO/GCE were not observed in PBS with and without H_2O_2. Only the Nf/Cyt *c*–VAErGO/GCE shows a clear H_2O_2 reduction

View Article Online
DOI: 10.1039/C7AN01387F

peak and the well-known peroxidase-like catalytic activity of immobilized Cyt *c* can be described by the following equations[38]

$$\text{Cyt } c - \text{Fe(III)} + e^- \rightarrow \text{Cyt } c - \text{Fe(II)}$$

$$2\text{Cyt } c - \text{Fe(II)} + 2H^+ + H_2O_2 \rightarrow 2\text{Cyt } c - \text{Fe(III)} + 2H_2O$$

Sensor characteristics and calibration curve for H_2O_2

In order to achieve optimum sensor performance conditions for the amperometric measurements of H_2O_2, the effects of pH and applied potential were investigated. The effect of solution pH was assessed in 100 μM H_2O_2 in 0.1 M PBS (pH 6.0–8.0) by using the Nf/Cyt *c*–VAErGO/GCE. After the addition of H_2O_2, the maximum amperometric response was obtained at pH 7.0 and this pH was chosen as the operating condition for the subsequent experiments. To optimize the applied potential, the measurements were repeated with 100 μM H_2O_2 using the Nf/Cyt *c*–VAErGO/GCE at the potential range from +0.2 V to −0.1 V. The results showed that no detectable current response of H_2O_2 was observed when the applied potential was higher than 0.1 V and the maximum response was obtained using a potential of –0.1 V. However, the time taken to achieve a stable baseline response was significantly decreased at 0.0 V and the reproducibility of response to H_2O_2 was also much greater. Because of these considerations, 0.0 V was used as the operating potential in all experiments.

To construct a calibration curve for H_2O_2 amperometric measurements were performed with different concentrations of H_2O_2 by using the Nf/Cyt *c*–VAErGO/GCE. Fig. 5A displays representative amperometric responses of H_2O_2 under the optimized experimental conditions. The current responses obtained reached maximum values in less than 15 s and each current response was measured 15 s after the addition of H_2O_2 samples. As shown in Fig. 5B, the H_2O_2 calibration curve was constructed and each error bar shown on the curve represents one standard

View Article Online
DOI: 10.1039/C7AN01387F

deviation over five measurements. In the curve obtained using the Nf/Cyt *c*–VAErGO/GCE, the equation of the regression line was calculated to be i (μA) = 3.289 C_{H2O2} (mM) – 0.0328 (R^2 = 0.993). The detection limit of the biosensor was taken as six times of the standard deviation of the current change due to the addition of a blank solution. Using the obtained calibration curve, the biosensor sensitivity was calculated to be 46.3 $\mu A \cdot mM^{-1} \cdot cm^{-2}$, the dynamic linear range was from 5.0 μM to 2.0 mM, and the detection limit was 2.3 μM (S/N = 3).

In order to investigate the performance characteristics of the biosensor, the data from the Nf/Cyt *c*–VAErGO/GCE system were compared with those from other relevant studies reported previously, and are summarized in Table 1. Although the present system shows a slightly lower detection limit, it operates at zero potential (0.0 V) and exhibits a higher sensitivity than the other methods listed. At a neutral operating potential and pH of our biosensor system, most interfering signals from in biological or clinical samples could be minimized or eliminated. The amperometric selectivity for the detection of H_2O_2 is often compromised by endogenous compounds such as ascorbic acid (AA), dopamine (DA), and glucose (Glu), which provide significant challenges for the detection of H_2O_2 in biological or clinical samples. Therefore, the H_2O_2-sensing ability of the Nf/Cyt *c*–VAErGO/GCE was investigated in the presence of these interfering species. The addition of 200 μM aliquots of AA, DA or Glu resulted in negligible interference when applying the potential at 0.0 V. In the present system, the additional Nafion layer of the Nf/Cyt *c*–VAErGO/GCE could prevent the cationic interferences such as AA. The biosensor also operated efficiently and in a repeatable manner as evidenced by the relative standard deviation (RSD) of 3.7 % (n = 5). The storage stability of the biosensor was examined by tracing the change in sensitivity of the electrodes response to 100 μM H_2O_2 over an extended

View Article Online
DOI: 10.1039/C7AN01387F

period. The Nf/Cyt *c*–VAErGO/GCE was stored at 4 °C in refrigerator. The biosensor showed that over 85% of their initial activity was retained after one-week storage.

In order to investigate the electrocatalytic activity of the immobilized Cyt *c* towards H_2O_2, the Michaelis-Menten equation[39] was applied and expressed in terms of current which was obtained from the calibration curve constructed. From the Lineweaver-Burk plot,[39] the maximum current density at substrate saturation (i_{max}) was calculated to be 219 $\mu A \cdot cm^{-2}$ and apparent Michaelis-Menton constant (K_m) was found to be 5.4 mM. The K_m value in the present study showed a significantly low value compared with other reports: adsorbed Cyt *c* on a screen printed graphite electrode[38] (230 mM) and on a thiol monolayer modified gold electrode[40] (144 mM). A small K_m value indicates a large binding affinity and the electrocatalytic reaction can reach half of i_{max} in a much lower H_2O_2 concentration.[39] Therefore, these results clearly demonstrate that an enhanced electrocatalytic activity and an increased affinity of the immobilized Cyt *c* towards H_2O_2.

Superoxide (SO) detection

From the studies reported previously, Cyt *c*[41,42] and superoxide dismutase (SOD)[43, 44] were widely used to construct the SO sensors. However, the SOD based approach has some practical limitations such as the amount of electron transfer from SO to electrode is decreased and uric acid interfering considerably. To overcome these issues, McNeil *et al.* have developed a SO sensor based on Cyt *c* immobilized on thiol modified gold electrodes to investigate the interaction of SO with Cyt *c* and the electrochemical properties of Cyt *c*.[45] By this approach, to improve the selectivity of their sensor, a low applied potential (+0.2 V) was used to eliminate the possible interferences. In our study, therefore, the amperometric detection of SO was carried out using the Nf/Cyt *c*–VAErGO/GCE under the optimized experimental conditions except the

View Article Online
DOI: 10.1039/C7AN01387F

applied potential was chosen as +0.2 V, which corresponds to the oxidation potential of Cyt *c*. The detection of SO is based on the redox reaction between the Cyt *c* immobilized on the surface of the GCE and the enzymatically generated SO.[28, 46, 47] Immobilized Cyt *c* in the Nf/Cyt *c*–VAErGO/GCE is reduced by SO and the reduced Cyt *c* is regenerated to its original state by electrochemically at the electrode surface.

As shown in Fig. 6, amperometric measurements of enzymatically generated SO were performed in 100 μM XA prepared in air-saturated 0.1 M PBS (pH 7.0). To detect SO, the Nf/Cyt *c*–VAErGO/GCE was used as a working electrode in the three electrode electrochemical cell set-up. After achieving a stable baseline current from 450 μL-volume of XA solution, a 50 μL aliquot of XOD samples was added. After the addition of a XOD sample, a noticeable change in current response was initiated immediately and the current change was monitored as a function of time (Fig. 6A).

As shown in Fig. 6B, a calibration curve for SO was constructed by plotting the current rate ($nA \cdot s^{-1}$) against the rate of SO production ($\mu M \cdot s^{-1}$) which was calculated from the XOD concentration by using a model study[47] due to difficulties in absolute measurements of SO concentration produced by the enzymatic reaction of XA with XOD. From the calibration curve, the detection limit of the designed biosensor was found to be 6.84 $nM \cdot s^{-1}$, linear range for the detection of SO was up to 1.44 $\mu M \cdot s^{-1}$ ($y = 0.439\ x - 0.175$, $R^2 = 0.961$), and the sensitivity was calculated to be 32.1 $\mu M \cdot nA^{-1} \cdot cm^{-2}$. This was compared with other SO sensors reported previously and summarized in Table 2. To confirm the SO detection process in our biosensor system, a well-known selective SO scavenger, SOD,[48] was used additional amperometric measurements. As can be seen in Fig. 6C, the amperometric current response of the Nf/Cyt *c*–VAErGO/GCE was increased by the addition of 4.0 μM XOD in 100 μM XA and the current

View Article Online
DOI: 10.1039/C7AN01387F

response was noticeably suppressed entirely until it reached the baseline signal upon the addition of 7.0 μM SOD. It shows that the enzymatically generated SO was completely inactivated by SOD. These results indicate that the signal is specific to SO radicals, without interference from the electrochemically active reaction by-product.

Conclusions

We have demonstrated the ability of an electrochemical biosensor to detect ROS, using Cyt *c* immobilized with VAErGO on a GCE surface. A simple "one step" electrodeposition method was applied to immobilize the Cyt *c* on the GCE surface. The VAErGO/GCE shows higher Cyt *c* loading efficiency and enhanced electro-catalytic activities towards H_2O_2 and SO. The Cyt *c* surface coverage (Γ) value was 1.03×10^{-10} mol·cm^{-2}, which is higher than the theoretical monolayer coverage value. The electrochemical results indicate that the immobilized Cyt *c* shows rapid (k_{et} value = 6.4 s^{-1}) and direct electron transfer properties. The higher sensitivity and selectivity was achieved for the amperometric H_2O_2 detection and enhanced catalytic activity of Cyt *c* towards H_2O_2 was observed (K_m value = 5.4 mM). The immobilized Cyt *c* exhibits peroxidase-like activity towards the reduction of H_2O_2 and an improved sensitivity to SO detection. Therefore, we conclude that the vertical alignment process of ErGO with Cyt *c* could be an excellent candidate for a new biosensor fabrication process and would be strongly applicable for the biological or clinical detection of ROS in *in vivo* and *in vitro* samples.

Acknowledgement

This work was supported by grant funding from the National Research Foundation of Korea (NRF) grant funded by the Korea government (MEST) (No. 2010-0005972) and the Pioneer

View Article Online
DOI: 10.1039/C7AN01387F

Research Center Program through the National Research Foundation of Korea funded by the Ministry of Science, ICT & Future Planning (MSIP) of Korea (NRF-2013M3C1A3065522).

View Article Online
DOI: 10.1039/C7AN01387F

References:

1. B. D'Autréaux and M. B. Toledano, *Nat. Rev. Mol. Cell Biol.*, 2007, **8**, 813-824.
2. H. J. Forman, M. Maiorino and F. Ursini, *Biochemistry (Mosc.)*, 2010, **49**, 835-842.
3. C. Nathan and A. Cunningham-Bussel, *Nat. Rev. Immunol.*, 2013, **13**, 349-361.
4. M. P. Murphy, *Biochem. J.*, 2009, **417**, 1-13.
5. M. Valko, D. Leibfritz, J. Moncol, M. T. D. Cronin, M. Mazur and J. Telser, *Int. J. Biochem. Cell Biol.*, 2007, **39**, 44-84.
6. R. Kohen and A. Nyska, *Toxicol. Pathol.*, 2002, **30**, 620-650.
7. A. Gomes, E. Fernandes and J. L. F. C. Lima, *J. Biochem. Biophys. Methods*, 2005, **65**, 45-80.
8. M. Kohno, *J. Clin. Biochem. Nutr.*, 2010, **47**, 1-11.
9. X. Chen, X. Tian, I. Shin and J. Yoon, *Chem. Soc. Rev.*, 2011, **40**, 4783-4804.
10. S. Borgmann, *Anal. Bioanal. Chem.*, 2009, **394**, 95-105.
11. P. Manning, C. J. McNeil, J. M. Cooper and E. W. Hillhouse, *Free Radic. Biol. Med.*, 1998, **24**, 1304-1309.
12. C. Calas□Blanchard, G. Catanante and T. Noguer, *Electroanalysis*, 2014, **26**, 1277-1286.
13. A. K. Yagati and J.-W. Choi, *Electroanalysis*, 2014, **26**, 1259-1276.
14. W. Chen, S. Cai, Q.-Q. Ren, W. Wen and Y.-D. Zhao, *Analyst*, 2012, **137**, 49-58.
15. L. Gorton, A. Lindgren, T. Larsson, F. D. Munteanu, T. Ruzgas and I. Gazaryan, *Anal. Chim. Acta*, 1999, **400**, 91-108.
16. M. Gómez-Mingot, J. Iniesta, V. Montiel, R. O. Kadara and C. E. Banks, *Analyst*, 2011, **136**, 2146-2150.
17. H. Ju, S. Liu, B. Ge, F. Lisdat and F. W. Scheller, *Electroanalysis*, 2002, **14**, 141-147.
18. P. S. Jensen, Q. Chi, F. B. Grumsen, J. M. Abad, A. Horsewell, D. J. Schiffrin and J. Ulstrup, *J. Phys. Chem. C*, 2007, **111**, 6124-6132.
19. A. B. Moghaddam, M. R. Ganjali, R. Dinarvand, T. Razavi, A. A. Saboury, A. A. Moosavi-Movahedi and P. Norouzi, *J. Electroanal. Chem.*, 2008, **614**, 83-92.
20. Q. Rui, K. Komori, Y. Tian, H. Liu, Y. Luo and Y. Sakai, *Anal. Chim. Acta*, 2010, **670**, 57-62.
21. G.-X. Wang, Y. Qian, X.-X. Cao and X.-H. Xia, *Electrochem. Commun.*, 2012, **20**, 1-3.
22. J. Wang, M. Li, Z. Shi, N. Li and Z. Gu, *Anal. Chem.*, 2002, **74**, 1993-1997.
23. J.-F. Wu, M.-Q. Xu and G.-C. Zhao, *Electrochem. Commun.*, 2010, **12**, 175-177.
24. N. Zhang, X. Lv, W. Ma, Y. Hu, F. Li, D. Han and L. Niu, *Talanta*, 2013, **107**, 195-202.
25. W. S. Hummers Jr and R. E. Offeman, *J. Am. Chem. Soc.*, 1958, **80**, 1339-1339.
26. F. Wang, Y. Wu, K. Lu, L. Gao and B. Ye, *Electrochim. Acta*, 2014, **141**, 82-88.
27. W. Ye, X. Zhang, Y. Chen, Y. Du, F. Zhou and C. Wang, *Int. J. Electrochem. Sci.*, 2013, **8**, 2122-2139.
28. X. J. Chen, A. C. West, D. M. Cropek and S. Banta, *Anal. Chem.*, 2008, **80**, 9622-9629.
29. A. Ambrosi, A. Bonanni and M. Pumera, *Nanoscale*, 2011, **3**, 2256-2260.
30. A. J. Bard and L. R. Faulkner, *Electrochemical methods: fundamentals and applications*, John Wiley & Sons, Inc., New York, 2nd edn., 2001.
31. V. Dharuman, J. H. Hahn, K. Jayakumar and W. Teng, *Electrochim. Acta*, 2013, **114**, 590-597.
32. X. Chen, R. Ferrigno, J. Yang and G. M. Whitesides, *Langmuir*, 2002, **18**, 7009-7015.
33. E. Laviron, *J. Electroanal. Chem.*, 1979, **100**, 263-270.
34. R. E. Dickerson, T. Takano, D. Eisenberg, O. B. Kallai, L. Samson, A. Cooper and E. Margoliash, *J. Biol. Chem.*, 1971, **246**, 1511-1535.
35. S. Alwarappan, R. K. Joshi, M. K. Ram and A. Kumar, *Appl. Phys. Lett.*, 2010, **96**, 263702.
36. M. Eguílaz, A. Gutiérrez and G. Rivas, *Sens. Actuators, B*, 2016, **225**, 74-80.
37. B. Dinesh, V. Mani, R. Saraswathi and S.-M. Chen, *RSC Adv.*, 2014, **4**, 28229-28237.
38. M. Gómez-Mingot, V. Montiel, C. E. Banks and J. Iniesta, *Analyst*, 2014, **139**, 1442-1448.

View Article Online
DOI: 10.1039/C7AN01387F

39. S. Casalini, G. Battistuzzi, M. Borsari, C. A. Bortolotti, G. Di Rocco, A. Ranieri and M. Sola, *J. Phys. Chem. B*, 2010, **114**, 1698-1706.
40. L. Wang and D. H. Waldeck, *J. Phys. Chem. C*, 2008, **112**, 1351-1356.
41. P. Rahimi, H. Ghourchian, H.A. Rafiee-Pour, *Analyst,* 2011, **136**, 3803–3808.
42. R. C. K. Wilson, D. T. Phuong, E. Chainani and A. Scheeline, *J. Electroanal. Chem.*, 2011, **662**, 100-104.
43. V. Lvovich and A. Scheeline, *Anal. Chem.*, 1997, **69**, 454-462.
44. V. Lvovich and A. Scheeline, *Anal. Chim. Acta*, 1997, **354**, 315-323.
45. C. J. McNeil, K. A. Smith, P. Bellavite and J. V. Bannister, *Free Radic. Res. Commun.*, 1989, **7**, 89-96.
46. S.-C. Chang, N. Pereira-Rodrigues, J. R. Henderson, A. Cole, F. Bedioui and C. J. McNeil, *Biosens. Bioelectron.*, 2005, **21**, 917-922.
47. K. Tammeveski, T. T. Tenno, A. A. Mashirin, E. W. Hillhouse, P. Manning and C. J. McNeil, *Free Radic. Biol. Med.*, 1998, **25**, 973-978.
48. M. Ganesana, J. S. Erlichman and S. Andreescu, *Free Radic. Biol. Med.*, 2012, **53**, 2240-2249.

View Article Online
DOI: 10.1039/C7AN01387F

Figure Captions

Scheme 1 Schematic representation of proposed H_2O_2 and SO biosensors based on Cyt *c* immobilized with VAErGO onto GCE.

Fig. 1 Typical AFM image of 3D view of (A) VAErGO and (B) Cyt *c*–VAErGO, height profiles obtained from solid line in the image of (C) VAErGO and (D) Cyt *c*–VAErGO.

Fig. 2 FE-SEM images of (A) VAErGO/ITO and (B) Cyt c–VAErGO/ITO. (C) Nyquist plots of (a) bare GCE, (b) VAErGO/GCE, and (c) Cyt c–VAErGO/GCE in 5 mM $[Fe(CN)_6]^{3-}$ (the dots represent the experimental and lines were theoretical fitting data's).

Fig. 3 (A) Cyclic voltammograms of (a) bare GCE, (b) Nf/VAErGO/GCE and (c) Nf/Cyt c–VAErGO/GCE in N_2-saturated 0.1 M PBS pH 7.0 at the scan rate of 100 $mV \cdot s^{-1}$ and (B) Cyclic voltammograms of Nf/Cyt c–VAErGO/GCE in 0.1 M PBS pH 7.0 at different scan rates ranged from 25 $mV \cdot s^{-1}$ to 200 $mV \cdot s^{-1}$.

Fig. 4 Cyclic voltammograms of (a) bare GCE, (b) Nf/VAErGO/GCE and (c) Nf/Cyt *c*–VAErGO/GCE in N_2-saturated 0.1 M PBS pH 7.0 without (dashed line) and with 500 µM H_2O_2 (solid line) at scan rate of 50 $mV \cdot s^{-1}$.

Fig. 5 (A) Representative amperometric responses of H_2O_2 (5.0 µM to 2.0 mM) on Nf/Cyt *c*–VAErGO/GCE (B) Calibration plot for H_2O_2 at applied potential of 0.0 V.

Fig. 6 (A) Amperometric response of SO produced by the enzymatic reaction of XA and XOD on the Nf/Cyt *c*–VAErGO/GCE, (B) SO calibration curve, and (C) amperometric response of the electrode for SO produced by the reaction of XA and XOD, and scavenging of produced SO by SOD at the potential of +0.2 V.

View Article Online
DOI: 10.1039/C7AN01387F

Scheme 1

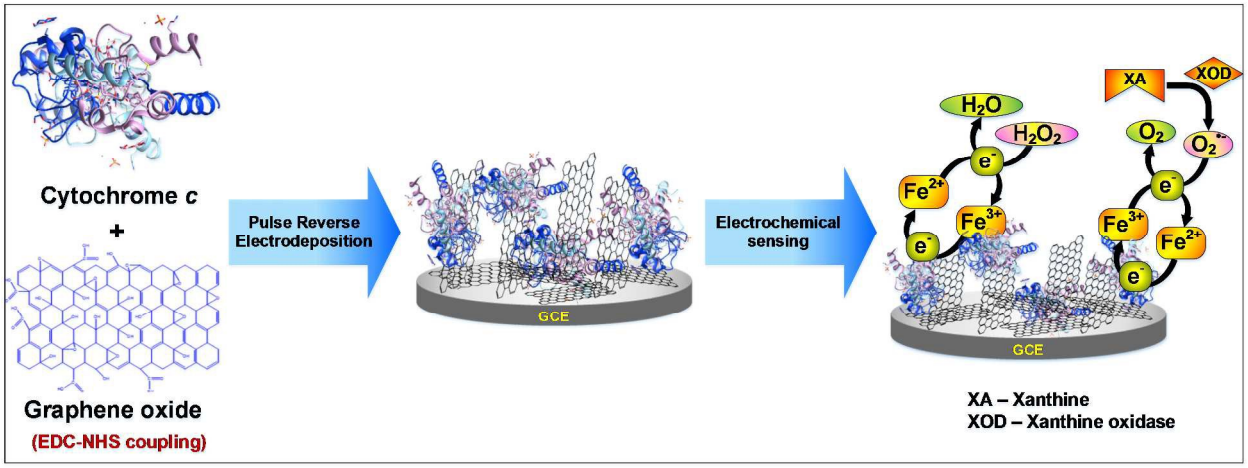

View Article Online
DOI: 10.1039/C7AN01387F

Fig. 1

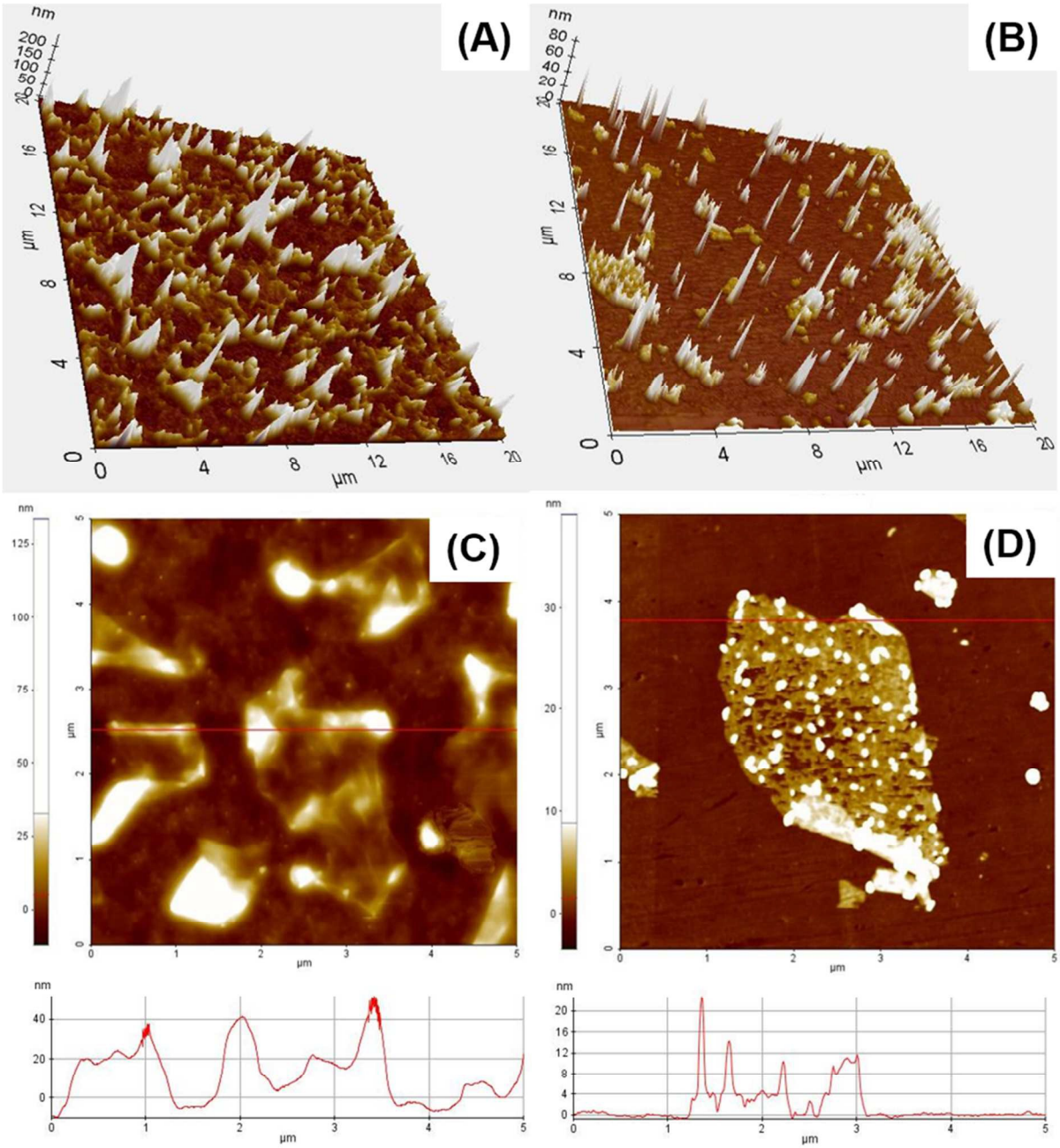

View Article Online
DOI: 10.1039/C7AN01387F

Fig. 2

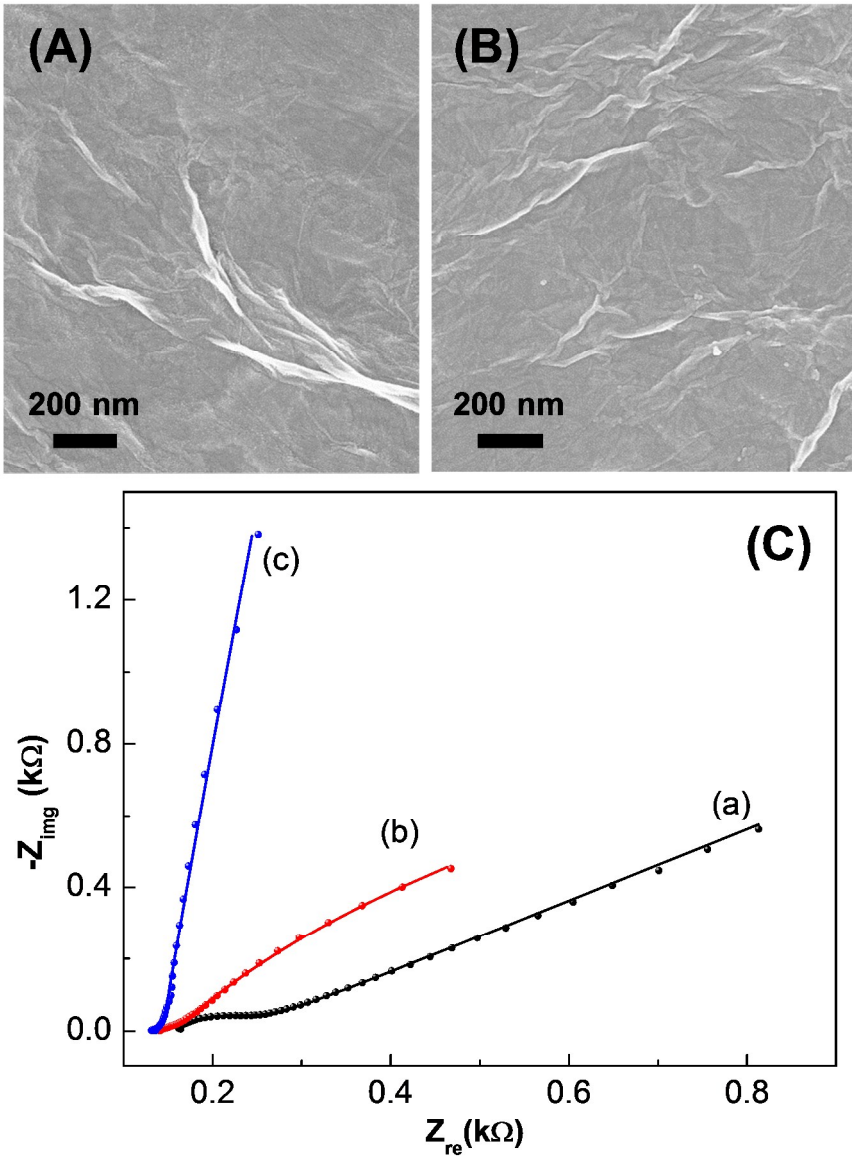

View Article Online
DOI: 10.1039/C7AN01387F

Fig. 3

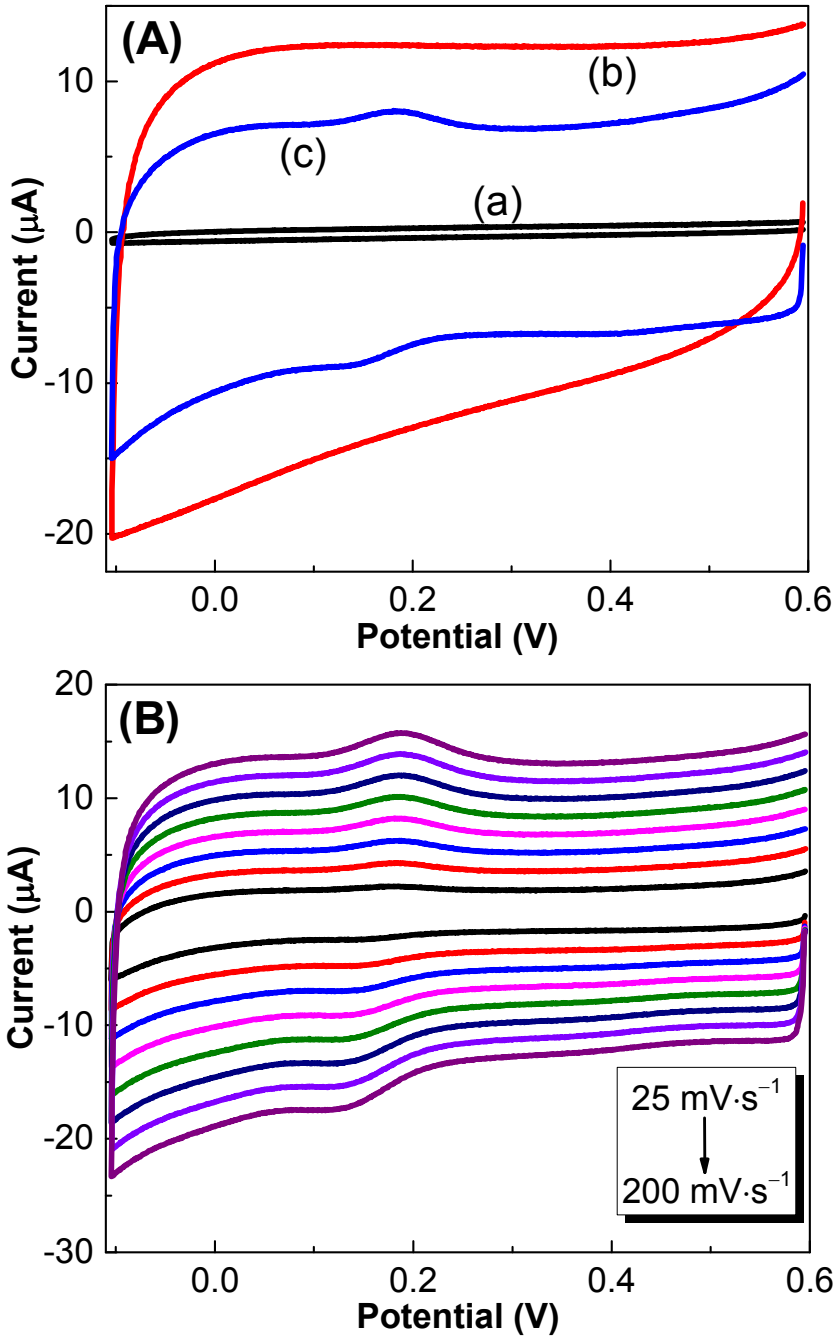

View Article Online
DOI: 10.1039/C7AN01387F

Fig. 4

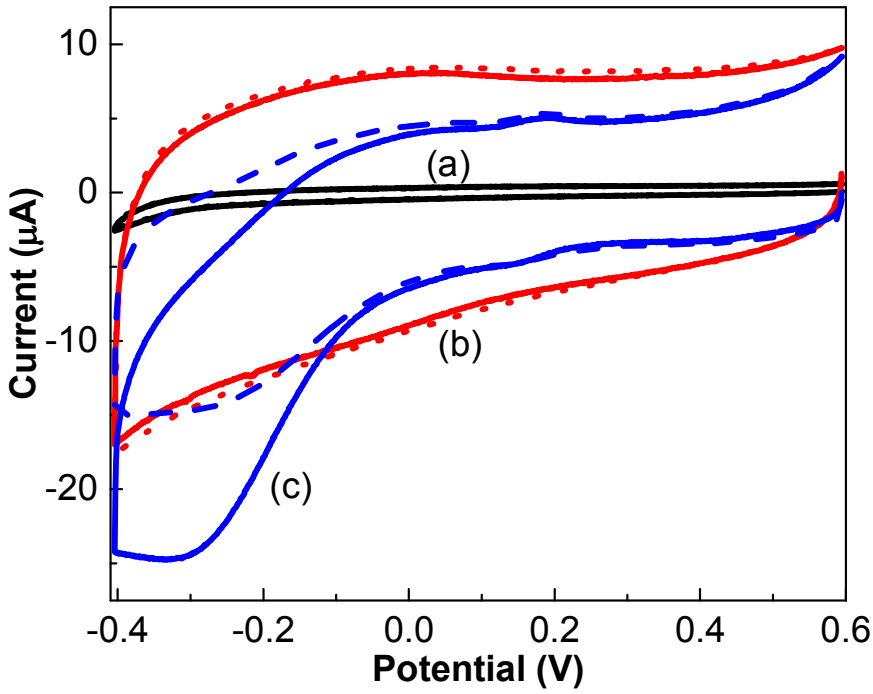

View Article Online
DOI: 10.1039/C7AN01387F

Fig. 5

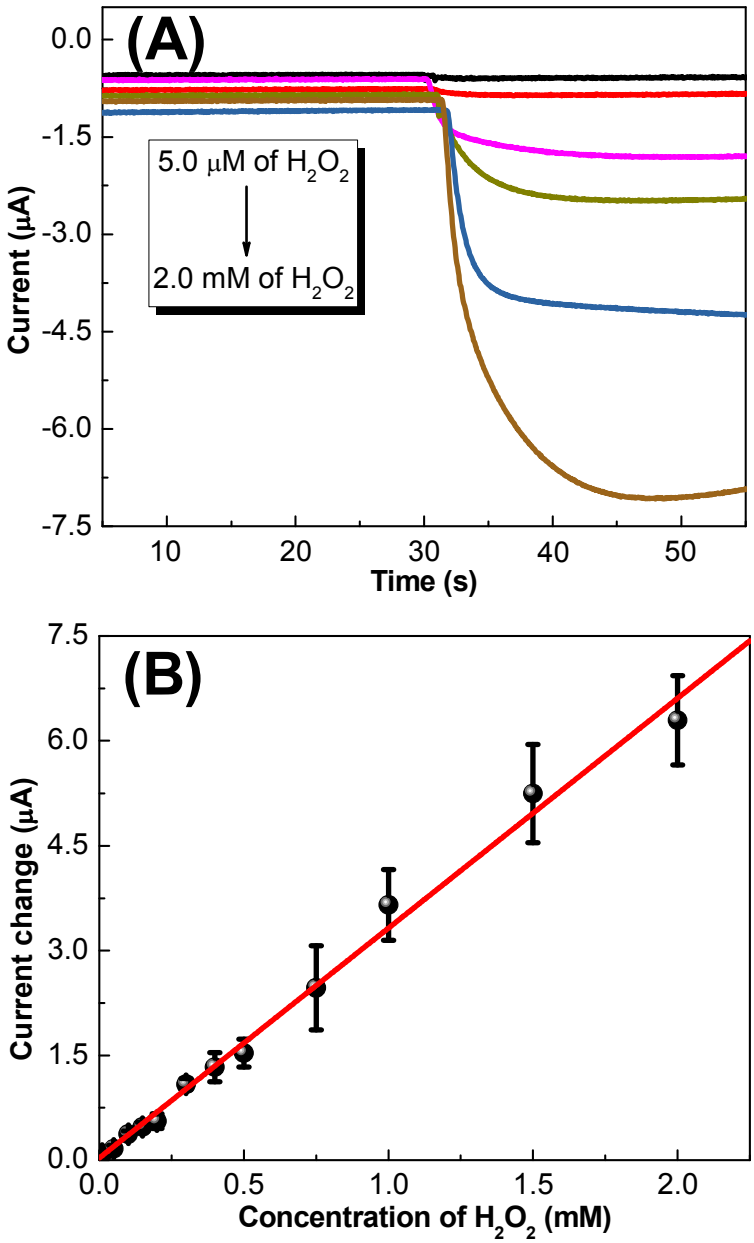

View Article Online
DOI: 10.1039/C7AN01387F

Fig. 6

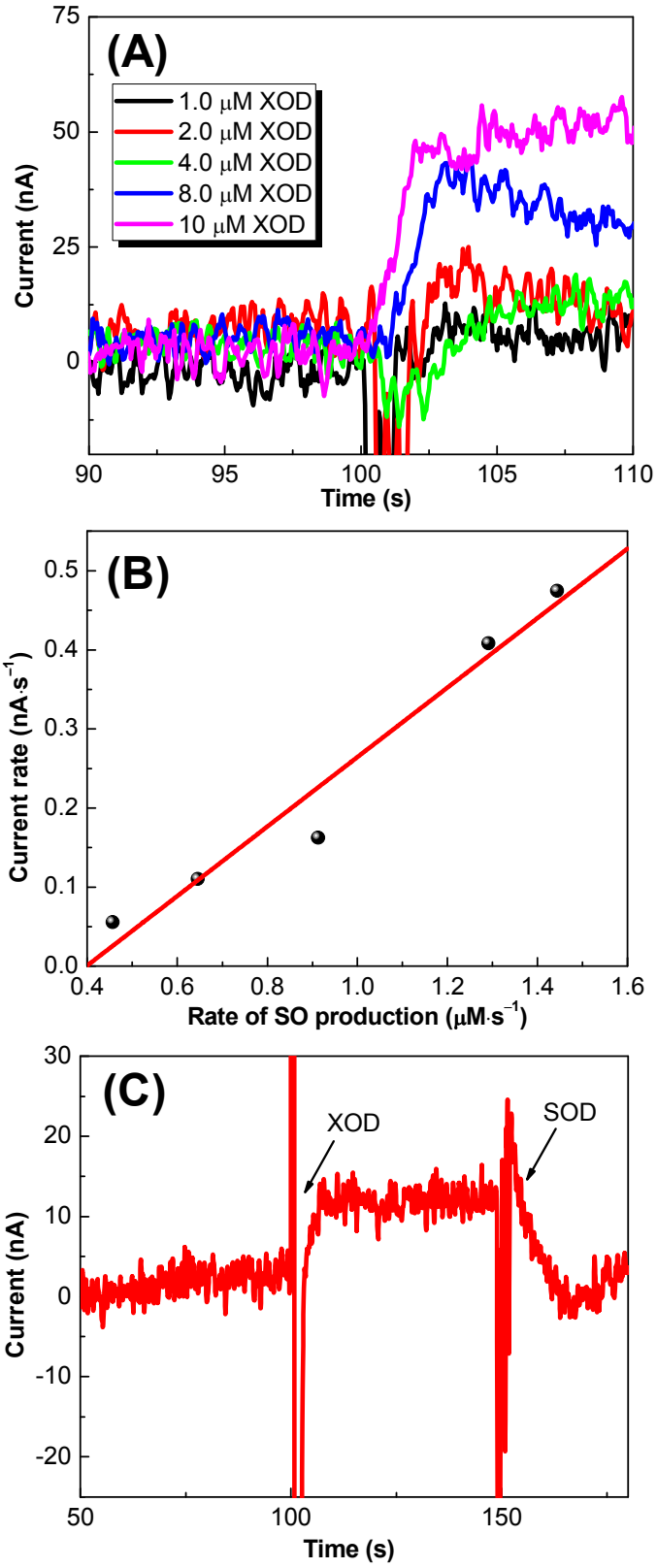

View Article Online
DOI: 10.1039/C7AN01387F

Table 1 Performance characteristics of Cyt *c* immobilized electrochemical sensors for H_2O_2.

Electrode materials	Operating potential (V *vs.* Ag/AgCl)	Sensitivity	LOD (μM)	Ref.
Cyt *c*–MWCNTs[a]/GCE	−0.10	43.0 μA·mM^{-1}·cm^{-2}	0.15	36
Cyt *c*/PTCA[b]–graphene/GCE	N/A	0.024 μA·mM^{-1}·cm^{-2}	3.5	24
Cyt *c*/G–PEDOT[c]/GCE	0.0	N/A	0.25	21
Nf/Cyt *c*–VAErGO/GCE	0.0	46.3 μA·mM^{-1}·cm^{-2}	2.3	This work

[a] Multi-walled carbon nanotubes. [b] 3,4,9,10-perylene tetracarboxylic acid. [c] Graphene/poly (3,4-ethylenedioxythiophene).

View Article Online
DOI: 10.1039/C7AN01387F

Table 2 Performance characteristics of Cyt *c* immobilized electrochemical sensors for SO.

Electrode materials	Operating potential (V *vs.* Ag/AgCl)	Sensitivity	LOD	Ref.
Cyt *c*/DTSP[a]/Au	+0.20	410 $nA \cdot \mu M^{-1} \cdot cm^{-2}$	73 nM	28
Cyt *c*/MU/MPA[b]/Au	+0.15	11.78×10^2 $\mu A \cdot \mu M^{-1} \cdot m^{-2}$	3.0 nM	48
Cyt *c*–RTIL[c]–MWCNTs/GCE	−0.50	7.455 $\mu A \cdot \mu M^{-1} \cdot cm^{-2}$	30 nM	41
Nf/Cyt *c*–VAErGO/GCE	+0.20	32.1 $\mu M \cdot nA^{-1} \cdot cm^{-2}$	6.84 $nM \cdot s^{-1}$	This work

[a] Dithiobis(succinimidyl)propionate. [b] 11-Mercaptoundecanoic acid/3-Mercaptopropionic acid. [c] Room temperature ionic liquid.